Extreme Mechanics Letters 56 (2022) 101841

Contents lists available at ScienceDirect

Extreme Mechanics Letters

journal homepage: www.elsevier.com/locate/eml

3D Kirigami antennas with robust frequency for stretchable wireless communication

Zhijian Wang [a,1], Hairui Wang [b,1], Fei Liu [c], Yu Kang [a], Ying Chen [a,c,*], Xue Feng [b,**]

[a] Jiaxing Key Laboratory of Flexible Electronics based Intelligent Sensing and Advanced Manufacturing Technology, Institute of Flexible Electronics Technology of THU, Zhejiang, Jiaxing, 314006, China
[b] AML, Department of Engineering Mechanics, Center for Flexible Electronics Technology, Tsinghua University, Beijing, 100084, China
[c] Qiantang Science and Technology Innovation Center, Hangzhou 310016, China

ARTICLE INFO

Article history:
Received 20 April 2022
Received in revised form 12 June 2022
Accepted 12 July 2022
Available online 25 July 2022

Keywords:
Stretchable electronics
Stretchable antenna
Kirigami
3D buckling
Flexible printed circuit board

ABSTRACT

Antenna, which is the essential electric component for wireless signal communication, requires one fixed electrical size for the stable working frequency. However, the frequency of the existing flexible antenna varies with its changing deformation, which leads to the loss of data packet or even transmission failure. Hence the fixed size of the existing flexible antenna is severely inconsistent with the deformation of flexible substrate. Here we propose a strategy to design and fabricate stretchable antennas with robust frequency based on three dimensional (3D) Kirigami, which is lightweight and deformation insensitive. With Kirigami design and assembling in 3D style, the radiation element of the antenna is mostly detached and strain-isolated from the soft substrate. Thus, not only bending, stretching and, compressing, but also the random dynamic disturbance deviates the resonant frequency little from the designed frequency in the wind disturbing experiments, as shown in the wind experiments It exhibits a superior strain insensitivity compared with the stretchable antennas ever reported. With mechanics guided design, the antenna's property remains stable after 5000 cycles bending deformation in the fatigue tests. Besides, an omnidirectionally stretchable and fully integrated device featured Bluetooth wireless communication enabled by 3D Kirigami antenna (2.45 GHz) has been designed and fabricated. Results show that the stretchable antenna strategy based on 3D Kirigami is robust for wearable electronics' wireless transmission.

1. Introduction

Flexible and stretchable electronics, that are deformable and can be integrated with human body in a comfortable way, have been attracting wide attention in skin-like and wearable physiological parameters monitoring [1–6]. Wireless signal transmission of the flexible electronics would be extremely important to realize the monitoring and facilitate the users in a continuous and decent way [7–12]. Antenna, as an essential component for wireless signal communication, needs one robust resonant frequency (RF) by keeping a constant electrical size [13,14]. Generally, the traditional antenna for the robust RF requires a rigid geometrical shape to maintain a constant electrical size in free space. However, the rigid shape is difficult to adapt to the stretching and bending deformation of human skin.

In order to fit the malleable human skin, many efforts have been devoted into flexible and stretchable antenna, which can be generally divided into two categories, i.e., unconventional material-based antennas [15–19] and mechanics designed ones [20–22]. The unconventional antennas fabricated by liquid metal and flexible dielectric material displays an excellent flexibility and stretchability [13,23]. The mechanics-designed antennas based on metal-serpentine, metal-mesh, and 3D helical assembly show the flexibility and stretchability in 2D/3D space [24–28]. However, the properties of these flexible antennas emerge massive variation including RF, bandwidth, and quality factor and etc. since their electrical sizes change with a large bending or stretching deformation of the changing substrate [29–33]. Generally, electromagnetic properties of antennas are dependent on not only the shape and physical dimension [34,35], but also the material characteristics [36]. The wearable devices integrated with flexible antenna usual attach on different substrates with a low profile, such as different parts of the human body and variant

* Corresponding author at: Jiaxing Key Laboratory of Flexible Electronics based Intelligent Sensing and Advanced Manufacturing Technology, Institute of Flexible Electronics Technology of THU, Zhejiang, Jiaxing, 314006, China.
** Corresponding author.
E-mail addresses: chenying@ifet-tsinghua.org (Y. Chen), fengxue@tsinghua.edu.cn (X. Feng).
[1] These authors contributed equally.

https://doi.org/10.1016/j.eml.2022.101841
2352-4316/

material surfaces whose permittivity, permeability, and conductivity will influence the RF, bandwidth, impedance matching and so on [37–39], making the electromagnetic properties deviated from the design. On the other hand, the larger bandwidth flexible antenna [25] has been designed to deal with the RF deviation, yet the performance on skin is weakened compared to that in air. The near-field communication (NFC) antenna with serpentines on the flexible substrate [40] could work normally under a large deformation of the skin with the RF excursion of only 0.3 MHz, yet the small bandwidth and gain limit the transmission speed and distance. All in all, two challenges to existing flexible antennas are that: (1) their RF vary with the changing geometry of the flexible electronics. (2) their RF are sensitive to the different permittivity of substrate materials. These would seriously decrease the wireless transmission of the wearable devices so far as to result in the loss of signal packet or transmission failure. Therefore, it becomes extremely important to solve the requiring contradiction between the constant size and RF and the stretching deformation, variant materials.

The fixed size of the existing flexible antenna for one stable RF is severely inconsistent with the large deformation of flexible substrate. The stability and reliability of RF becomes a serious problem that affects the performance of the flexible electronic during the stretching and bending of the human body. Recently, Kirigami and 3D buckling assembling methods with highly reliable packaging [41–43] provides a useful prospect for designing new structures and solving the above two problems of flexible antennas. The working principle is that Kirigami design and 3D buckling assembling render the radiation element of the antenna distanced from the soft substrate with small strain inside during bending, stretching, and compressing. The antenna possesses RF stability under a large deformation, insensitivity to the substrate materials. Systematic simulations and experiments have been carried out to verify these designs. What is more, an omnidirectionally stretchable and fully integrated device featured with signal sensing, data collecting and processing, and Bluetooth wireless communication functions has been designed and built to further demonstrate the practical utility of this strategy. Hopefully, the 3D Kirigami antenna with constant RF can help realizing more wearable and stretchable electronics with good wireless communication ability.

2. Structural design of 3D Kirigami antenna

A skin-like electronic device works on a human body where is a dynamically deformable environment enriched with bending, stretching, wind disturbing and so on. As shown in Fig. 1(a), the physiological data like body temperature, heart rate, electrocardiograph (ECG), blood glucose, movement velocity, etc. shall be wirelessly transmitted via the antenna. Traditional flexible printed circuit (FPC) antennas with a solid form fail to accommodate the deformable substrate and work properly. For the above problems, we propose a substrate materials and strain insensitive 3D Kirigami antenna to solve the dilemma of deformation and stable RF.

As shown in the upper right of Fig. 1(a), Kirigami technology has been introduced in the design of a Kirigami antenna fed by coplanar waveguide (CPW) which is made from polyimide (PI) film with copper. The antenna precursor is composed of ground plane, radiating element, flexible substrate and cutting gap, in which the radiating element is isolated from the flexible substrate by the cutting gap. With compressive buckling method, the flat precursor can be buckled in the out-of-plane direction as a 3D Kirigami antenna. Then the 3D Kirigami antenna can be stretched or compressed on any stretchable substrate. Most importantly, the radiating element in the antenna remains undeformed with little strain during stretching, compressing and bending deformation, which ensures its RF stable. Based on the Kirigami antenna strategy, a series of antenna with different structural units have been designed as shown in Fig. 2(a).

The dielectric constant of the 3D Kirigami structure is determined by the stretchable substrate, PI and air. According to the serial mixing model [44], the dielectric constant of the composite material could be estimated,

$$\varepsilon_r^{-1} = \sum_i V_i \varepsilon_i^{-1} \tag{1}$$

where ε_r is the dielectric constant of the composite material. V_i and ε_i are the volume percentage and dielectric constant of the ith phase, respectively.

Since the air dielectric constant is 1, the dielectric constant ε_r shall be determined by the volume percentages and dielectric constants of the PI and PDMS films. As can been seen from Fig. 1(a), the thickness of the composite is equal to the displacement of the antenna film based on the buckling theory [45] as,

$$u(x) = \frac{1}{2}\sqrt{\frac{4\delta L}{\pi^2} - \frac{4h^2}{3}}\left(1 + \cos\frac{2\pi x}{L}\right) \tag{2}$$

where L is the length of the 2D antenna precursor before buckling. δ is the antenna's ends horizontal displacement. h is the thickness of the PI.

Then the sectional area of the air part could be evaluated as,

$$\begin{aligned} S &= \int_{-0.5L+\delta}^{0.5L-\delta} u(x)dx \\ &= \sqrt{\frac{4\delta L}{\pi^2} - \frac{4h^2}{3}}\{(0.5L-\delta) + \sin[\frac{2\pi}{L}(0.5L-\delta)]\} \end{aligned} \tag{3}$$

Defining the width of PI as W, the volume of air part (V) could be expressed as,

$$V = W \cdot S \tag{4}$$

In this research, we assume that the PI and PDMS films have same volume that is 192 mm^3. The dielectric constants of PI and PDMS films are 3.5 and 2.8, respectively. According to the Eq. (1), the variation volume percentages of the PI, PDMS and air are the primary contribution to the dielectric constant ε_r. Once the antenna is bulked into 3D state, the air volume percentage will increase quickly and become the main component, leading to the dielectric constant ε_r of near 1 as can been seen from table S1, which has also displayed the horizontal displacement δ and volume of air part at different applied strains. Thus, this structure will offer a stable dielectric constant ε_r for the dielectric material of the antenna even under large deformation, and then make the approximated effective dielectric constant (ε_{eff}) keep a stable value.

3. Frequency robustness of Kirigami antenna

Here we use 100 μm thickness PI film as the flexible substrate and 18 μm thickness copper as the radiating element of 1-unit-cake 3D Kirigami antenna. And the compressive buckling of 1the 3D Kirigami antenna is conducted by releasing the substrate with previous applied strain (AS). AS = 100% presents that the antenna is as unstretched as the originally designed 3D state. AS = 0% indicates that the antenna is ultimately stretched into flat state as the 2D precursor. 3D Kirigami antennas' return losses with and without substrate have been numerically calculated under different stretching deformation. Fig. 1(b) shows the return losses of a free-standing 3D Kirigami antenna, whose maximum RF deviation is only 0.043 GHz. The reason is shown in the inset, i.e., the maximum principal strain in the metal is 0.8% at the leg

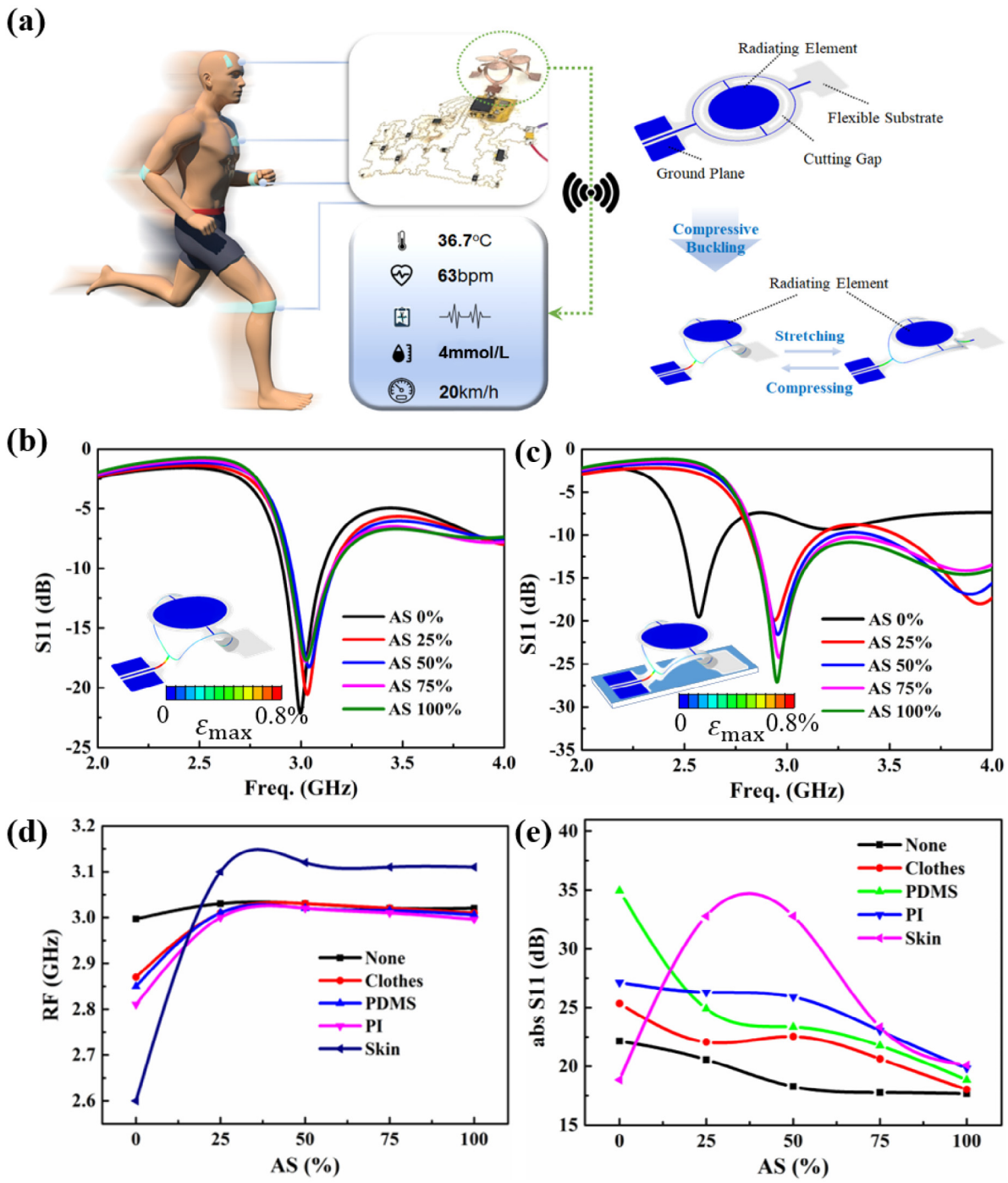

Fig. 1. Motivation and antenna structure designs. (a) Background and the Kirigami antenna fed by CPW, composed of ground plane, radiating element, flexible substrate and cutting gap. (b) S_{11} results of 1-unit-cake antenna without PDMS substrate under different ASs, and the inset is the FEM analysis result under 100% AS. (c) S_{11} results of the 3D Kirigami antenna adhered on a polydimethylsiloxane (PDMS) substrate under different ASs. (d) The effects of different kinds of adherend substrates on the RF of the 3D Kirigami antenna. (e) S_{11} results of the 3D Kirigami antenna with different kinds of adherend substrates.

and the radiating element moves like a rigid body in the space as design experiencing nearly zero strain. Fig. 1(c) shows the return losses of a 3D Kirigami antenna on a stretchable substrate (made of polydimethylsiloxane, PDMS). The RF of 3D antennas (AS $\neq$ 0%) are stable during stretching, which is desired in the stretchable devices. And there is an obvious RF transition (i.e., a deviation of 0.427 GHz) between limit 2D state (AS = 0%) and the other 3D states. The RF transition here is a general microprint of 2D antenna's performance dependence on substate materials. Because the permittivity of PDMS (∼2.8) is larger than that of the air (∼1) [18], the RF of the 2D antenna shifts to lower frequency compared to the 3D antenna. The corresponding direction diagrams been displayed in figure S1, in which the shape and beam pointing of the 3D antennas (with/without stretchable substrate) are similar other than the 2D ones.

The radiating element's detaching from the stretchable substrate in the 3D Kirigami antenna not only makes its RF irrelevant from the deformation transmitted by the stretchable substrate, but also renders its RF independent from the substrate's permittivity. Commonly used flexible or stretchable substrate (e.g., clothes, PDMS, PI and skin) enabled 3D Kirigami antennas have been simulated as shown in Fig. 1(d). It turns out that

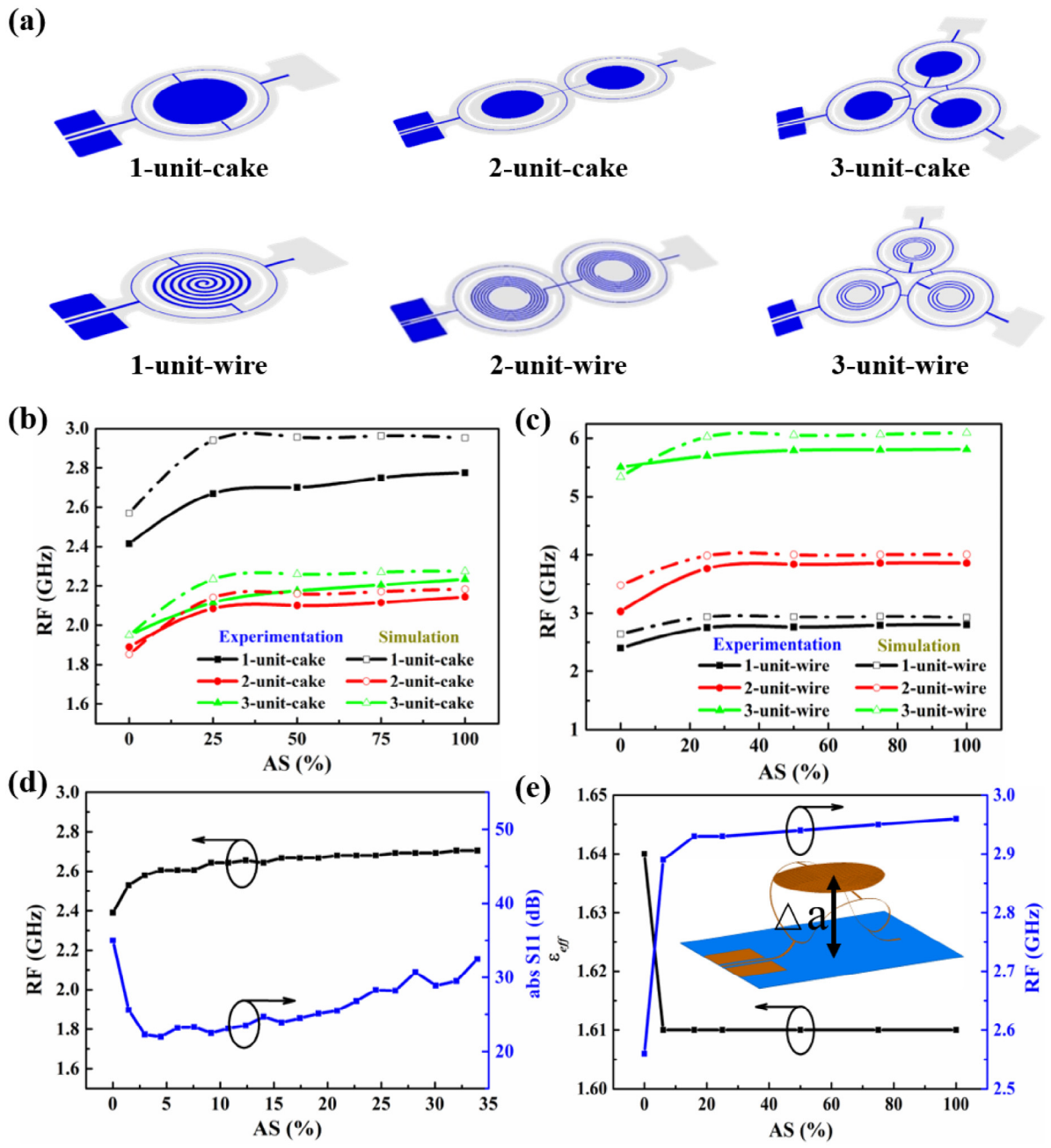

Fig. 2. Simulations and measurements results of antennas with different kinds of structures. (a) Antenna 2D precursor. (b) Simulated and experimental results of the resonant frequencies for the antennas. (c) Simulated and experimental results of the S_{11} for the antennas. (d) The detailed RF results of 1-unit-cake antenna by experimental measurement. (e) The ε_{eff} and RF of 1-unit-cake antenna under different ASs with PDMS adherend substrate.

the RF at AS = 0% is different for disparate substrate, since the antenna is attached on the substrate. Yet, due to the radiating element's detachment to the substrate, the RF keeps similar and unchanged at the 3D state where AS > 0%. As shown in Fig. 1(e), the absolute values of the return losses are all larger than 10 dB, whose variation could be attributed to the impedance matching induced by the substrates and the antenna shapes. Thus, the results revealed that 3D Kirigami could make traditional FPC antennas display a favorable stretchability and a well substrate-and deformation-independent RF property.

To further confirm 3D Kirigami antenna strategy could improve the stability of the RF, a series of antennas with different structural units in Fig. 2(a) have been analyzed by the finite element method (FEM). All the 3D Kirigami antennas with different units and patterns possess small maximum principal strain (< 1%) even at 100% AS, as seen from table S2. Then these antennas are imported into the HFSS code to design and simulate their electromagnetic property. The antenna precursors are fabricated by FPC technology and 3D assembled by compressive buckling with the AS of the stretchable substrate, as shown in table S3. The simulated and experimental results of the RF during stretching deformation are shown in Fig. 2(b) and (c). It turns out that the experimental results are accord with the simulated ones. The RF of these Kirigami antennas is insensitivity to the deformation.

The absolute values of the return losses for all the antennas are higher than 10 dB, as shown in figure S2(a) and (b), and the simulated gains shown in figure S2(c) are greater than 0 dBi, indicating all the antennas could receive and transmit signals. Besides, the aforementioned transition and 3D antenna's stable RF are also observed here, indicating that the 3D Kirigami antenna

strategy can be effective in more other designs with different radiating elements and different RFs. Table S4 shows different kinds of antennas with their RF, RF deviation, RF offset, flexibility and Stretchability. The results shows that the 3D Kirigami antennas possess a better RF-stability property with a relatively low RF deviation and offset.

To further investigate the RF transition between 2D and 3D antenna, experiment with smaller deformation steps has been conducted as shown in Fig. 2(d). The antenna's RF (denoted as f_r) can be empirically predicted by the following equation [46,47],

$$f_r \approx \frac{c}{\sqrt{\varepsilon_{eff}} \times L_{ant}} \tag{5}$$

where c and ε_{eff} are the speed of light in free space and the approximated effective permittivity, respectively, and L_{ant} is the length of the antenna. According to the Eq. (5), the RF for the determined radiating element's pattern is mainly dependent on the approximated effective permittivity. Take the 3D Kirigami antenna (PDMS substrate, RF = 3 GHz) in the inset of Fig. 2(e) as an example, in view of the irregular structure and electromagnetic simulation without the consideration of the buckling PI film, the approximated effective permittivity is simulated by HFSS as shown in Fig. 2(e). When the radiating element gets detached from the soft substate with the increasing AS, the air part is added on the substrate, causing the approximated effective permittivity decreases sharply at the transition phase. Thus, the RF increases rapidly meanwhile. This result is agreement with the material structure design. After buckling and leaving from the substrate, the metal layer which displays a very low strain contributes to an approximately equal resistance. In addition, the load impedances of all the buckling antennas belong to inductive impedance at their RFs according to the Smith chart, as shown in figure S3(a). Thus, all the antennas could be equivalent to a serial circuit, composed of a resistance and an inductance, which has been shown in figure S3(b). For all the buckling antennas, the inductances are mainly influenced by the metal layer size and retain a similar result. Both the similar resistance and inductance lead to a constant RF for the buckling antennas.

Besides, these antennas' bending behaviors have also been studied by bending them onto different radius. Antenna on non-pre-strained substrate is stable in RF during bending with an obvious transition (RF deviation = 0.143 GHz) in plane and curvy as shown in figure S4. However, the antenna whose radiating element is detached from the pre-strained substrate is stable in RF from plane to curvy as shown in figure S5, and the RF deviation is only 0.06 GHz. Thus, the 3D Kirigami antenna is able to keep stable RF during stretching and bending deformation till the radiating element touch the substrate.

Moreover, the repeated deformation may cause metal or plastic fatigue in the antenna and degenerate its performance. Thus, the fatigue resistance evaluation of the 3D Kirigami antennas have been carried out by the tensile and compression test systems (Care Measurement and Control, China) as shown in figure S6. The fatigue test has been shown in video S1. The place with the biggest strain in the antenna is highlighted in Fig. 3(a), which exhibits no crack or delamination-like differences after 5000 cycles stretching deformation as shown by the before and after scanning electron microscope images in Fig. 3(b) and Fig. 3(c), respectively. Meanwhile, the antenna is connected to the network analyzer by a high frequency test line, and the return losses of plane antenna and 3D Kirigami antenna are tested and recorded every 1000 cycles. As shown in Fig. 3(d) and (e), the RF changes little indicating the 3D Kirigami antenna is fatigue friendly.

To examine the antenna's RF stability in dynamic deformation occasion, the wind disturbance experiments of three typical designs have been conducted as shown in video S2(a) ~(c). The blower with randomly changing wind direction acts as the dynamic deformation loader. And the return loss is in situ and in real time measured. As demonstrated in Fig. 3(f), the 3D Kirigami antenna involves large deformation under wind blast. Comparing the three typical deformations at the bottom of Fig. 3(f), the RF is relatively stable at the designed value and the return losses are lower than −10 dB, as shown in Fig. 3(g), indicating its ability to transmit electromagnetic radiation effectively during randomly deformed conditions.

4. Application for wireless communication

To further demonstrate the feasibility of this strategy, we have designed a stretchable and flexile integrated device with functions including sensing, data processing and wireless communication by Bluetooth, whose circuit layout is shown in Fig. 4(a). Connection lines between two components adopt serpentine lines in the circuit. The relative distance increase in the circuit between the two components, which can withstand more deformation and improve its extensibility. The analog temperature signal captured by the sensor is converted into digital signal by the analog digital converter (ADC) and processed in the microcontroller unit (MCU) before transmitted to the mobile phone by the antenna as shown in Fig. 4(b). A mobile phone application is developed to display the signal and the RSSI (Received Signal Strength Indicator). A 4-cake patterned 3D Kirigami antenna and serpentine interconnects are used to enable the omnidirectional stretchability. The 4-cake patterned 3D Kirigami antenna's maximum principal strain during 30% stretching and compressing is below 0.72% as calculated in the figure S7.

Then the integrated device with 3D Kirigami antenna is fabricated by laser cutting (DL300U, China) and transfer printing. As shown in figure S8, the fabrication is started with laminating FCCL (Flexible Copper Clad Laminate) onto a silicone layer and patterning them into antenna precursor by laser cutting. And the 3D Kirigami antenna is assembled by compressive buckling after the extra FCCL is removed. Meanwhile the fabricated FPCB is laminated onto a silicone layer and patterned into a stretchable network similarly. Then the patterned FPCB network is transferred onto a water-soluble tape with its circuit facing upside, before Ecoflex is blade coated on it. After the Ecoflex is cured and the water-soluble tape is resolved, the chips are assembled onto the stretchable circuits together with the antenna whose RF is 2.45 GHz. The final product is shown in Fig. 4(c), and it can be bent and stretched easily. Before testing the stretchable integrated device, the Bluetooth antenna's performance during deformation has been numerically calculated where the stretchable circuit has been considered as the ground plane as shown in the inset of Fig. 4(d). Results show that the antenna's RF is stable at the designed value during 30% stretching deformation as shown in Fig. 4(d), other than the RF transition in 2D and 3D state as aforementioned.

To test the 3D Kirigami antenna integrated device under deformation, it is attached onto a balloon as shown in Fig. 5(a). By inflation (i.e., $\triangle V > 0$) and deflation (i.e., $\triangle V < 0$), the device is stretched or compressed omnidirectionally on the spherical surface where the serpentine interconnects are expanded or curved and the 3D Kirigami antenna is flattened or arched up. Meanwhile the RSSI is recorded to evaluate the quality of the wirelessly communicated data. Here, the Bluetooth chip's RSSI working range is from 0 to −93 dBm. Results show that the RSSI keeps around −40 dBm during 30% stretching deformation indicating the 3D Kirigami antenna's good performance during stretching and compressing. The details can be found in Video S3(a). We have also attached the 3D Kirigami antenna onto human's arm as displayed in Fig. 5(c). A stable RSSI of about −71.8 dBm is obtained in the

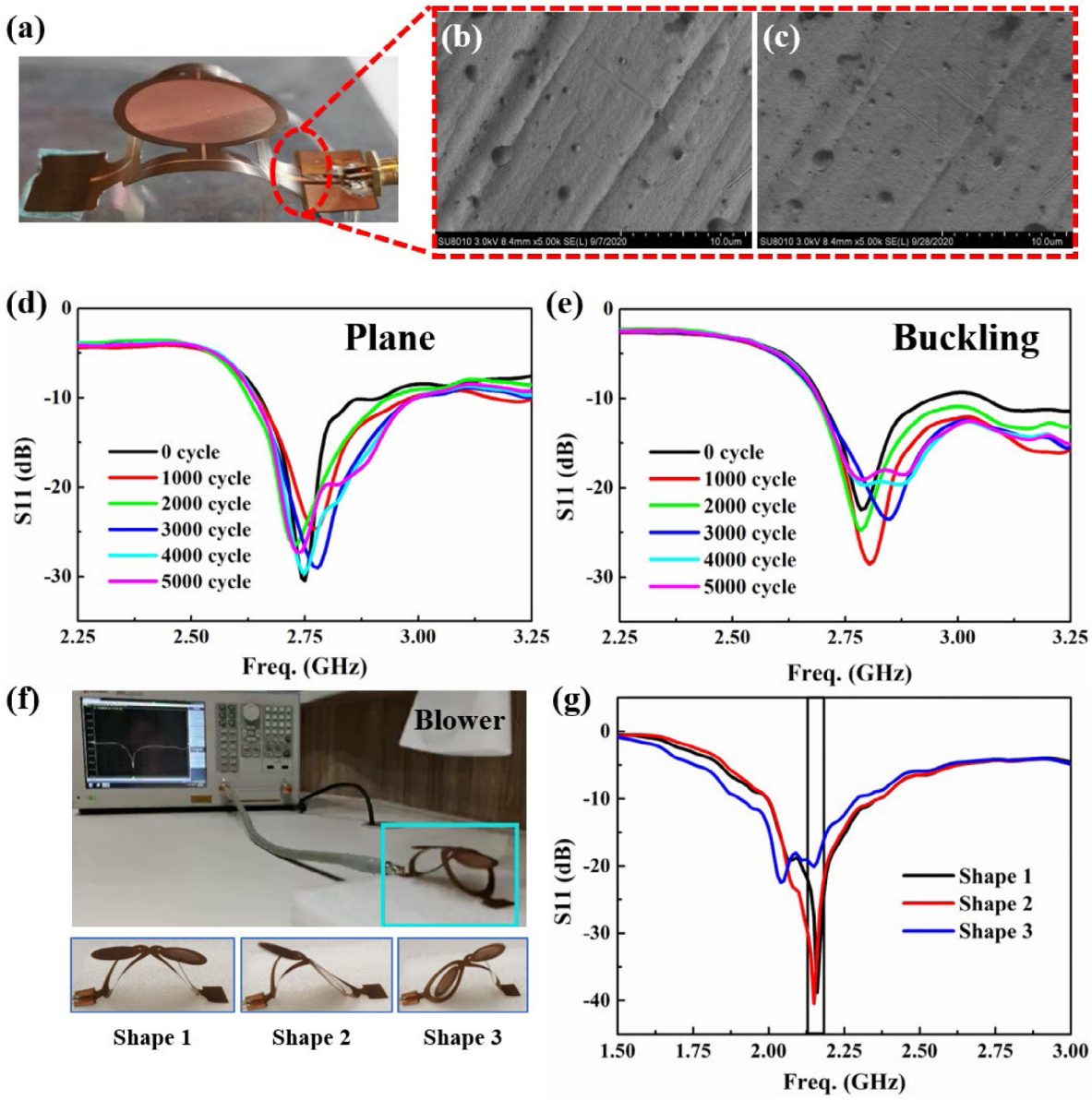

Fig. 3. Fatigue resistance analysis of the 3D Kirigami antennas. (a) The 3D Kirigami antenna for 1-unit-cake antenna. (b) and (c) the microstructures of the copper at the position of maximum principal strain of 1-unit-cake antenna before and after the 5000 cycles fatigue resistance measurements, respectively. (d) and (e) S_{11} results of 1-unit-cake antenna in 2D and 3D state under different fatigue cycles, respectively. (f) 3D 2-unit-cake antenna under wind blowing. (g) S_{11} results of the antenna at different shapes.

process of the arm rotation and antenna deformation, shown in Fig. 5(d) and Video S3(b). In addition, we have also tested the working distance of this antenna with this integrated device as shown in Fig. 5(e). The RSSI decreases when the device is getting away from the mobile phone, and keeps within the acceptable range (i.e., 0 to −93 dBm) within the distance of 80 m, as shown in Fig. 5(f). In addition, the mobile phone has been receiving the signal data within a distance of 140 m as shown in Video S3(c), indicating that the 3D Kirigami antenna has a well far-field communication property.

5. Conclusions

In conclusion, the antenna's performance under deformation circumstances determines flexible and stretchable electronics' quality in data wireless communication. Here we propose a strategy to design a stretchable and robust RF antenna by Kirigami. These flexible and stretchable antennas are insensitive to substrate deformation as well as the substrate material category, since the radiating elements are detached from the substrate during working. These antennas can be freely bent and conformal to planar, non-planar and deformable structures. The RF stable mechanism has been analyzed by the combined mechanics and electromagnetic simulation based on FEM. Different kinds of antenna designs have been simulated, measured during stretching, compressing and bending deformation. The results indicate that within the deformation limit in which the radiating element touches the soft substrate, the RF of the 3D Kirigami antenna shall well keep relatively unchanged. Besides, this 3D Kirigami antenna can be simply made of FPCB materials and easily fabricated by laser cutting and compressive buckling assembling, which is highly accommodated with the method in fabricating flexible circuits. Furthermore, the feasibility has been demonstrated by designing a 3D Kirigami Bluetooth antenna and integrated which

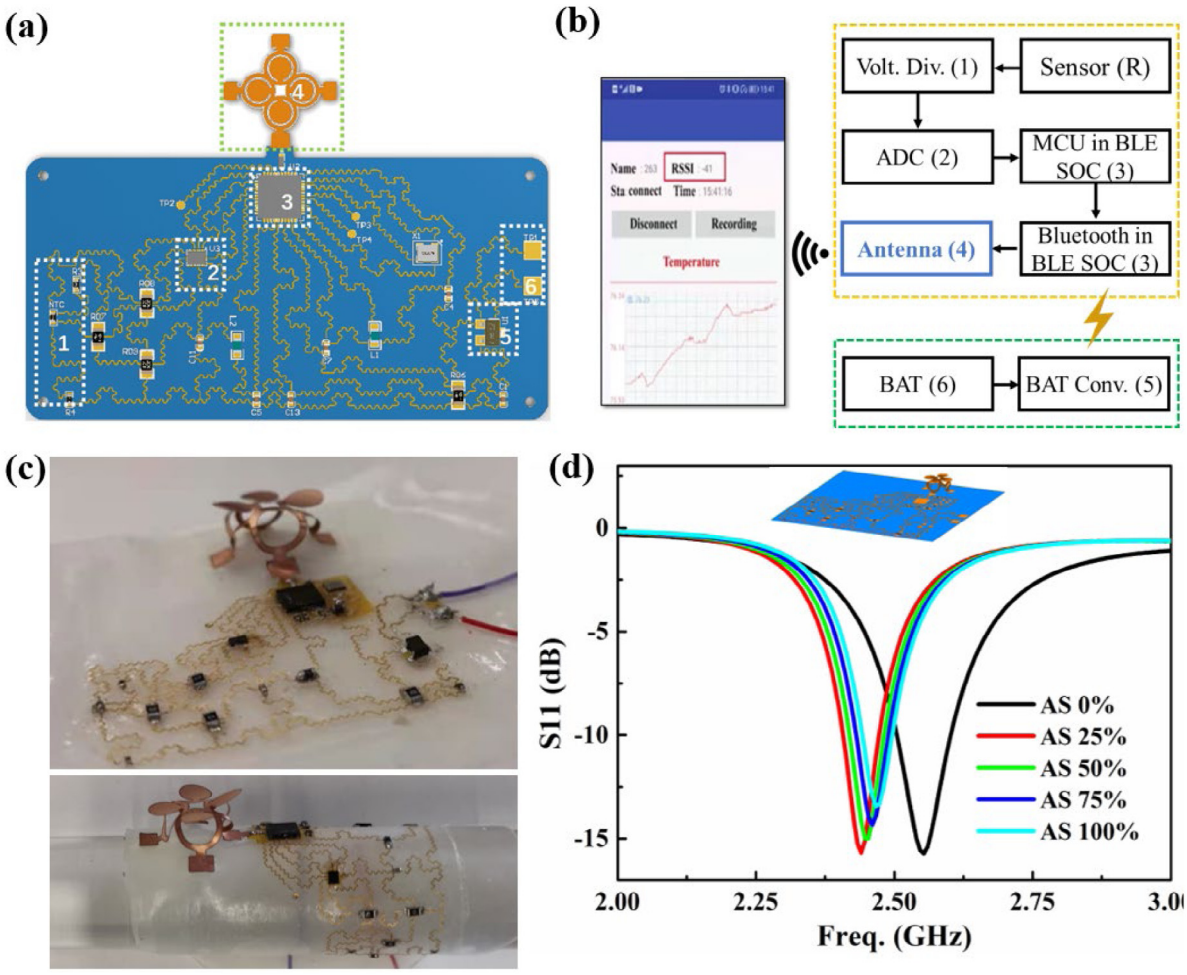

Fig. 4. Bluetooth antenna design and fabrication. (a) and (b) the circuit structure and principle diagram, respectively. (c) The final product of stretchable circuits. (d) S_{11} simulation results of the 4-unit-cake antenna. The inset is the model.

with an omnidirectional stretchable circuit. The transmission signal quality and the acceptable wireless communication distance have been tested. It turns out that the 3D Kirigami design not only enables antenna's stable RF during deformation, but also helps improving the acceptable distance for wireless communication in a stretchable integrated device. The Kirigami designed method for 3D Kirigami antenna with constant frequency can help realizing more wearable and stretchable electronics with good wireless communication.

6. Experimental section

6.1. 3D Kirigami antenna's mechanics and electromagnetic simulation

The finite element methods were adopted in mechanics simulation and electromagnetic simulation. The 3D Kirigami antenna's assembling process and stretching deformation are statically simulated by the commercial software ABAQUS. The maximum principal strain was chosen to estimate the strain state of radiating element during deformation. Eight-node 3D solid elements (C3D8R) and four-node shell elements (S4R) were used to simulate the silicone substrate and 2D precursors, respectively. The elastic modulus (E) and Poisson's ratio (ν) are $E_{\text{substrate}} = 166$ kPa, $\nu_{\text{substrate}} = 0.49$, $E_{\text{Cu}} = 117$ GPa, $\nu_{\text{Cu}} = 0.34$, $E_{\text{PI}} = 2.5$ GPa, $\nu_{\text{PI}} = 0.34$. On the other hand, the electromagnetic simulation of reflection coefficient (S_{11}) characteristics of the antennas is simulated by commercial code ANSYS HFSS. The 3D configurations of these antenna were given by the mechanics simulations. Then it was imported in to the HFSS and fed by coplanar waveguide (CPW). The relative permittivity (ε_r), relative permeability (μ_r), and conductivity (σ) are $\varepsilon_{r\_Cu} = 1$, $\mu_{r\_Cu} = 0.999991$, $\sigma_{Cu} = 5.8 \times 10^7$ S m^{-1}, $\varepsilon_{r\_substrate} = 3.5$, $\mu_{r\_substrate} = 1$, $\sigma_{\text{substrate}} = 2.5 \times 10^{-14}$ S m^{-1}. It was focused on the radiation characteristics, such as resonant frequencies of antennas under the different deformation states. Meanwhile, the antenna size was optimized according to the frequency requirements in the design. A flexible copper clad laminate with 100 μm-thick PI film and 18 μm-thick copper was used to prepare the Kirigami antennas by the flexible printed circuit technology. The 4-unit-cake antenna for the Bluetooth application in the flexible electronic system (FES) was cut by a laser device (DL300U).

6.2. The stretchable integrated device with bluetooth antenna

The circuit was shown in Fig. 4(a). Component 1 was an NTC (Negative Temperature Coefficient) thermistor, which could directly convert temperature change into resistance change. The AD chip converted the analog resistive signal into digital signal and transmitted which to a microcontroller unit (MCU, component 3) chip. This SoC chip was integrated with a Bluetooth inside, and sent the processed data to a mobile phone application through the 3D Kirigami Bluetooth antenna. The temperature signal was displayed on the phone. Component 5 was an N-type triode protecting the circuit. Component 6 was a power input

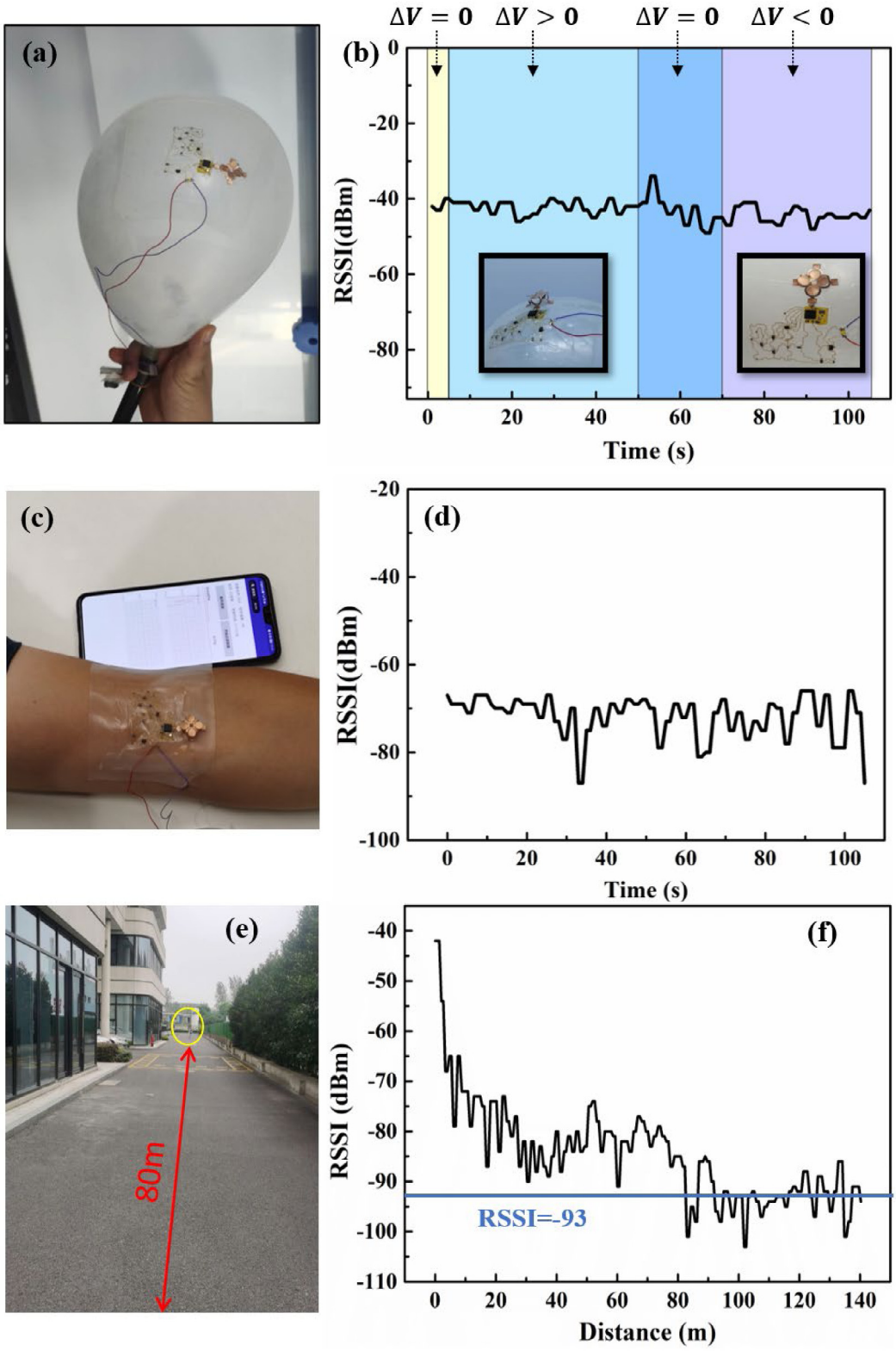

Fig. 5. Application analysis of the Bluetooth antenna in the stretchable circuits. (a) The stretchable circuits attached to a balloon. (b) RSSI results of the stretchable circuits on the balloon under different volume states. (c) The stretchable circuits attached to human's arm. (d) RSSI results of the stretchable circuits on human's arm. (e) RSSI-distance test of the stretchable circuits. (f) RSSI results at different distances.

pin. To enable the stretchability of the circuits, the serpentine interconnects were especially used. What is more, to make the stretchable circuits in a single layered FPCB, the zero-ohm resistor was adopted where the interconnects crossed in. The fabrication of the stretchable circuits began with laminating a 100 μm thick PI sheet onto the substrate before deposition of copper (18 μm) by the plating. Then the metal layers were patterned by photolithography and wet etching based on the designed serpentine

circuit. The PI sheet patterned into the serpentine circuit was attached to a prepared Ecoflex (1.5 mm thickness). The serpentine circuit was cut by the laser machine to strip the extra PI film beside the serpentine interconnects. The cut circuit was transferred on to a water-soluble tape and covered by Ecoflex before curing in a vacuum drying oven at 80 °C for 2 h. Then the hydrosol was washed off via the deionized water. Chips, battery and 3D Kirigami antenna were integrated on the circuit through solder.

The circuit is connected to the mobile phone through the app, and the 5-inch balloon was inflated by 20%. Relying on the Van der Waals' force, the prepared circuit was attached on the surface of the balloon. Compressed air was filled into the balloon via an air gun. The wirelessly transmitted signal was recorded in real time during the balloon expansion process. Temperature signal data was recorded in real time when the inflated balloon was rotated in three directions.

Declaration of competing interest

The authors declare that they have no known competing financial interests or personal relationships that could have appeared to influence the work reported in this paper.

Data availability

Data will be made available on request.

Acknowledgments

This work was supported by the Zhejiang Province Key Research and Development Project, China (Grant No. 2019C05002, 2020C05004, 2021C01183), National Natural Science Foundation of China (Grant No. U20A6001, 11902292, 12102223) and Postdoctoral program of Zhejiang province, China (Grant No. ZJ2020018).

Appendix A. Supplementary data

Supplementary material related to this article can be found online at https://doi.org/10.1016/j.eml.2022.101841.

References

[1] J.A. Rogers, T. Someya, Y. Huang, Materials and mechanics for stretchable electronics, Science 327 (2010) 1603–1607, http://dx.doi.org/10.1126/science.1182383.

[2] T.R. Ray, J. Choi, A.J. Bandodkar, S. Krishnan, P. Gutruf, L. Tian, R. Ghaffari, J.A. Rogers, Bio-integrated wearable systems: A comprehensive review, Chem. Rev. 119 (2019) 5461–5533, http://dx.doi.org/10.1021/acs.chemrev.8b00573.

[3] Y. Chen, S. Lu, S. Zhang, Y. Li, Z. Qu, Y. Chen, B. Lu, X. Wang, X. Feng, Skin-like biosensor system via electrochemical channels for noninvasive blood glucose monitoring, Sci. Adv. 3 (2017) e1701629, http://dx.doi.org/10.1126/sciadv.1701629.

[4] H. Li, Y. Xu, X. Li, Y. Chen, Y. Jiang, C. Zhang, B. Lu, J. Wang, Y. Ma, Y. Chen, Y. Huang, M. Ding, H. Su, G. Song, Y. Luo, X. Feng, Epidermal inorganic optoelectronics for blood oxygen measurement, Adv. Healthc. Mater. 6 (2017) 1601013, http://dx.doi.org/10.1002/adhm.201601013.

[5] F. Zhu, H. Xiao, H. Li, Y. Huang, Y. Ma, Irregular hexagonal cellular substrate for stretchable electronics, J. Appl. Mech. 86 (2019) http://dx.doi.org/10.1115/1.4042288.

[6] J. Wu, M. Li, W. Chen, D. Kim, Y. Kim, Y. Huang, K. Hwang, Z. Kang, J.A. Rogers, A strain-isolation design for stretchable electronics, Acta Mech. Sinica-PRC 26 (2010) 881–888, http://dx.doi.org/10.1007/s10409-010-0384-x.

[7] J. Kim, A. Banks, H. Cheng, Z. Xie, S. Xu, K. Jang, J.W. Lee, Z. Liu, P. Gutruf, X. Huang, P. Wei, F. Liu, K. Li, M. Dalal, R. Ghaffari, X. Feng, Y. Huang, S. Gupta, U. Paik, J.A. Rogers, Epidermal electronics with advanced capabilities in near-field communication, Small 11 (2015) 906–912, http://dx.doi.org/10.1002/smll.201402495.

[8] H. Li, Y. Ma, Z. Liang, Z. Wang, Y. Cao, Y. Xu, H. Zhou, B. Lu, Y. Chen, Z. Han, S. Cai, X. Feng, Wearable skin-like optoelectronic systems with suppression of motion artifacts for cuff-less continuous blood pressure monitor, Natl. Sci. Rev. 7 (2020) 849–862, http://dx.doi.org/10.1093/nsr/nwaa022.

[9] W. Gao, S. Emaminejad, H.Y.Y. Nyein, S. Challa, K. Chen, A. Peck, H.M. Fahad, H. Ota, H. Shiraki, D. Kiriya, D. Lien, G.A. Brooks, R.W. Davis, A. Javey, Fully integrated wearable sensor arrays for multiplexed in situ perspiration analysis, Nature 529 (2016) 509–514, http://dx.doi.org/10.1038/nature16521.

[10] Y. Chen, Y. Zhang, Z. Liang, Y. Cao, Z. Han, X. Feng, Flexible inorganic bioelectronics, Npj Flex. Electron. 4 (2020) http://dx.doi.org/10.1038/s41528-020-0065-1.

[11] Y. Chen, B. Lu, D. Ou, X. Feng, Mechanics of flexible and stretchable piezoelectrics for energy harvesting, Sci. China Phys. Mech. 58 (2015) http://dx.doi.org/10.1007/s11433-015-5692-5.

[12] Y. Ma, Y. Zhang, S. Cai, Z. Han, X. Liu, F. Wang, Y. Cao, Z. Wang, H. Li, Y. Chen, X. Feng, Flexible hybrid electronics for digital healthcare, Adv. Mater. 32 (2020) 1902062, http://dx.doi.org/10.1002/adma.201902062.

[13] J. So, J. Thelen, A. Qusba, G.J. Hayes, G. Lazzi, M.D. Dickey, Reversibly deformable and mechanically tunable fluidic antennas, Adv. Funct. Mater. 19 (2009) 3632–3637, http://dx.doi.org/10.1002/adfm.200900604.

[14] F. Liu, X. Cheng, F. Zhang, Y. Chen, H. Song, Y. Huang, Y. Zhang, Design and assembly of reconfigurable 3D radio-frequency antennas based on mechanically triggered switches, Adv. Electron. Mater. 5 (2019) 1900256, http://dx.doi.org/10.1002/aelm.201900256.

[15] D. Tang, Q. Wang, Z. Wang, Q. Liu, B. Zhang, D. He, Z. Wu, S. Mu, Highly sensitive wearable sensor based on a flexible multi-layer graphene film antenna, Sci. Bull. 63 (2018) 574–579, http://dx.doi.org/10.1016/j.scib.2018.03.014.

[16] Z. Wang, P. Li, R. Song, W. Qian, H. Zhou, Q. Wang, Y. Wang, X. Zeng, L. Ren, S. Yan, S. Mu, D. He, High conductive graphene assembled films with porous micro-structure for freestanding and ultra-low power strain sensors, Sci. Bull. 65 (2020) 1363–1370, http://dx.doi.org/10.1016/j.scib.2020.05.002.

[17] B.S. Kim, K. Shin, J.B. Pyo, J. Lee, J.G. Son, S. Lee, J.H. Park, Reversibly stretchable, optically transparent radio-frequency antennas based on wavy Ag nanowire networks, ACS Appl. Mater. Inter. 8 (2016) 2582–2590, http://dx.doi.org/10.1021/acsami.5b10317.

[18] A.S.M. Alqadami, B. Mohammed, K.S. Bialkowski, A. Abbosh, Fabrication and characterization of flexible polymer iron oxide composite substrate for the imaging antennas of wearable head imaging systems, IEEE Antenn. Wirel. Pr. 17 (2018) 1364–1368, http://dx.doi.org/10.1109/LAWP.2018.2841879.

[19] Y.H. Jung, J. Lee, Y. Qiu, N. Cho, S.J. Cho, H. Zhang, S. Lee, T.J. Kim, S. Gong, Z. Ma, Stretchable twisted-pair transmission lines for microwave frequency wearable electronics, Adv. Funct. Mater. 26 (2016) 4635–4642, http://dx.doi.org/10.1002/adfm.201600856.

[20] Z. Xie, R. Avila, Y. Huang, J.A. Rogers, Flexible and stretchable antennas for biointegrated electronics, Adv. Mater. 32 (2020) 1902767, http://dx.doi.org/10.1002/adma.201902767.

[21] T. Pan, M. Pharr, Y. Ma, R. Ning, Z. Yan, R. Xu, X. Feng, Y. Huang, J.A. Rogers, Experimental and theoretical studies of serpentine interconnects on ultrathin elastomers for stretchable electronics, Adv. Funct. Mater. 27 (2017) 1702589, http://dx.doi.org/10.1002/adfm.201702589.

[22] T. Chang, Y. Tanabe, C.C. Wojcik, A.C. Barksdale, S. Doshay, Z. Dong, H. Liu, M. Zhang, Y. Chen, Y. Su, T.H. Lee, J.S. Ho, J.A. Fan, A general strategy for stretchable microwave antenna systems using serpentine mesh layouts, Adv. Funct. Mater. 27 (2017) 1703059, http://dx.doi.org/10.1002/adfm.201703059.

[23] S. Cheng, Z. Wu, P. Hallbjorner, K. Hjort, A. Rydberg, Foldable and stretchable liquid metal planar inverted cone antenna, IEEE Trans. Antennas and Propagation 57 (2009) 3765–3771, http://dx.doi.org/10.1109/TAP.2009.2024560.

[24] J. Zhang, R. Song, X. Zhao, R. Fang, B. Zhang, W. Qian, J. Zhang, C. Liu, D. He, Flexible graphene-assembled film-based antenna for wireless wearable sensor with miniaturized size and high sensitivity, ACS Omega 5 (2020) 12937–12943, http://dx.doi.org/10.1021/acsomega.0c00263.

[25] E. Thangaselvi, K. Meena Alias Jeyanthi, Implementation of flexible denim nickel copper rip stop textile antenna for medical application, Cluster. Comput. 22 (2019) 635–645, http://dx.doi.org/10.1007/s10586-017-1647-0.

[26] F. Liu, Y. Chen, H. Song, F. Zhang, Z. Fan, Y. Liu, X. Feng, J.A. Rogers, Y. Huang, Y. Zhang, High performance, tunable electrically small antennas through mechanically guided 3D assembly, Small 15 (2019) 1804055, http://dx.doi.org/10.1002/smll.201804055.

[27] J. Zhu, J.J. Fox, N. Yi, H. Cheng, Structural design for stretchable microstrip antennas, ACS Appl. Mater. Inter. 11 (2019) 8867–8877, http://dx.doi.org/10.1021/acsami.8b22021.

[28] K. Li, X. Cheng, F. Zhu, L. Li, Z. Xie, H. Luan, Z. Wang, Z. Ji, H. Wang, F. Liu, Y. Xue, C. Jiang, X. Feng, L. Li, J.A. Rogers, Y. Huang, Y. Zhang, A generic soft encapsulation strategy for stretchable electronics, Adv. Funct. Mater. 29 (2019) 1806630, http://dx.doi.org/10.1002/adfm.201806630.

[29] Z. Yan, F. Zhang, F. Liu, M. Han, D. Ou, Y. Liu, Q. Lin, X. Guo, H. Fu, Z. Xie, M. Gao, Y. Huang, J. Kim, Y. Qiu, K. Nan, J. Kim, P. Gutruf, H. Luo, A. Zhao, K. Hwang, Y. Huang, Y. Zhang, J.A. Rogers, Mechanical assembly of complex, 3D mesostructures from releasable multilayers of advanced materials, Sci. Adv. 2 (2016) e1601014, http://dx.doi.org/10.1126/sciadv.1601014.

[30] A.M. Hussain, F.A. Ghaffar, S.I. Park, J.A. Rogers, A. Shamim, M.M. Hussain, Metal/polymer based stretchable antenna for constant frequency far-field communication in wearable electronics, Adv. Funct. Mater. 25 (2015) 6565–6575, http://dx.doi.org/10.1002/adfm.201503277.

[31] F. Xu, H. Zhu, Y. Ma, Y. Qiu, Electromagnetic performance of a three-dimensional woven fabric antenna conformal with cylindrical surfaces, Text. Res. J. 87 (2017) 147–154, http://dx.doi.org/10.1177/0040517515624878.

[32] Y. Ma, K. Jang, L. Wang, H.N. Jung, J.W. Kwak, Y. Xue, H. Chen, Y. Yang, D. Shi, X. Feng, J.A. Rogers, Y. Huang, Design of strain-limiting substrate materials for stretchable and flexible electronics, Adv. Funct. Mater. 26 (2016) 5345–5351, http://dx.doi.org/10.1002/adfm.201600713.

[33] G. Samanta, D. Mitra, Dual-band circular polarized flexible implantable antenna using reactive impedance substrate, IEEE Trans. Antennas and Propagation 67 (2019) 4218–4223, http://dx.doi.org/10.1109/TAP.2019.2905978.

[34] A.S.M. Alqadami, K.S. Bialkowski, A.T. Mobashsher, A.M. Abbosh, Wearable electromagnetic head imaging system using flexible wideband antenna array based on polymer technology for brain stroke diagnosis, IEEE Trans. Biomed. Circuits Syst. 13 (2019) 124–134, http://dx.doi.org/10.1109/TBCAS.2018.2878057.

[35] L. Song, A.C. Myers, J.J. Adams, Y. Zhu, Stretchable and reversibly deformable radio frequency antennas based on silver nanowires, ACS Appl. Mater. Inter. 6 (2014) 4248–4253, http://dx.doi.org/10.1021/am405972e.

[36] F. Mokhtari-Koushyar, P.M. Grubb, M.Y. Chen, R.T. Chen, A miniaturized tree-shaped fractal antenna printed on a flexible substrate: A lightweight and low-profile candidate with a small footprint for spaceborne and wearable applications, IEEE Antennas Propag. Mag. 61 (2019) 60–66, http://dx.doi.org/10.1109/MAP.2019.2907878.

[37] W. Yeo, Y. Kim, J. Lee, A. Ameen, L. Shi, M. Li, S. Wang, R. Ma, S.H. Jin, Z. Kang, Y. Huang, J.A. Rogers, Multifunctional epidermal electronics printed directly onto the skin, Adv. Mater. 25 (2013) 2773–2778, http://dx.doi.org/10.1002/adma.201204426.

[38] S. Sunwoo, K. Ha, S. Lee, N. Lu, D. Kim, Wearable and implantable soft bioelectronics: Device designs and material strategies, Annu. Rev. Chem. Biomol. 12 (2021) 359–391, http://dx.doi.org/10.1146/annurev-chembioeng-101420-024336.

[39] H. Li, Y. Ma, Y. Huang, Material innovation and mechanics design for substrates and encapsulation of flexible electronics: a review, Mater. Horiz. 8 (2021) 383–384, http://dx.doi.org/10.1039/d0mh00483a.

[40] Z. Li, T. Le, Z. Wu, Y. Yao, L. Li, M. Tentzeris, K. Moon, C.P. Wong, Rational design of a printable, highly conductive silicone-based electrically conductive adhesive for stretchable radio-frequency antennas, Adv. Funct. Mater. 25 (2015) 464–470, http://dx.doi.org/10.1002/adfm.201403275.

[41] K. Li, X. Cheng, F. Zhu, L. Li, Z. Xie, H. Luan, Z. Wang, Z. Ji, H. Wang, F. Liu, Y. Xue, C. Jiang, X. Feng, L. Li, J.A. Rogers, Y. Huang, Y. Zhang, A generic soft encapsulation strategy for stretchable electronics, Adv. Funct. Mater. 29 (2019) 1806630, http://dx.doi.org/10.1002/adfm.201806630.

[42] M. Han, H. Wang, Y. Yang, C. Liang, W. Bai, Z. Yan, H. Li, Y. Xue, X. Wang, B. Akar, H. Zhao, H. Luan, J. Lim, I. Kandela, G.A. Ameer, Y. Zhang, Y. Huang, J.A. Rogers, Three-dimensional piezoelectric polymer microsystems for vibrational energy harvesting, robotic interfaces and biomedical implants, Nat. Electron. 2 (2019) 26–35, http://dx.doi.org/10.1038/s41928-018-0189-7.

[43] S. Chen, Z. Liu, H. Du, C. Tang, C. Ji, B. Quan, R. Pan, L. Yang, X. Li, C. Gu, X. Zhang, Y. Yao, J. Li, N.X. Fang, J. Li, Electromechanically reconfigurable optical nano-kirigami, Nature Commun. 12 (2021) 1299, http://dx.doi.org/10.1038/s41467-021-21565-x.

[44] K. Wakino, T. Okada, N. Yoshida, K. Tomono, A new equation for predicting the dielectric constant of a mixture, J. Am. Ceram. Soc. 76 (1993) 2588–2594, http://dx.doi.org/10.1111/j.1151-2916.1993.tb03985.x.

[45] J. Song, Y. Huang, J. Xiao, S. Wang, K.C. Hwang, H.C. Ko, D.H. Kim, M.P. Stoykovich, J.A. Rogers, Mechanics of noncoplanar mesh design for stretchable electronic circuits, J. Appl. Phys. 105 (2009) 123516, http://dx.doi.org/10.1063/1.3148245.

[46] T. Ma, S. Wu, Ultrawideband band-notched folded strip monopole antenna, IEEE Trans. Antennas and Propagation 55 (2007) 2473–2479, http://dx.doi.org/10.1109/TAP.2007.904137.

[47] F. Zhu, S. Gao, A.T. Ho, R.A. Abd-Alhameed, C.H. See, T.W.C. Brown, J. Li, G. Wei, J. Xu, Multiple band-notched UWB antenna with band-rejected elements integrated in the feed line, IEEE Trans. Antennas and Propagation 61 (2013) 3952–3960, http://dx.doi.org/10.1109/TAP.2013.2260119.